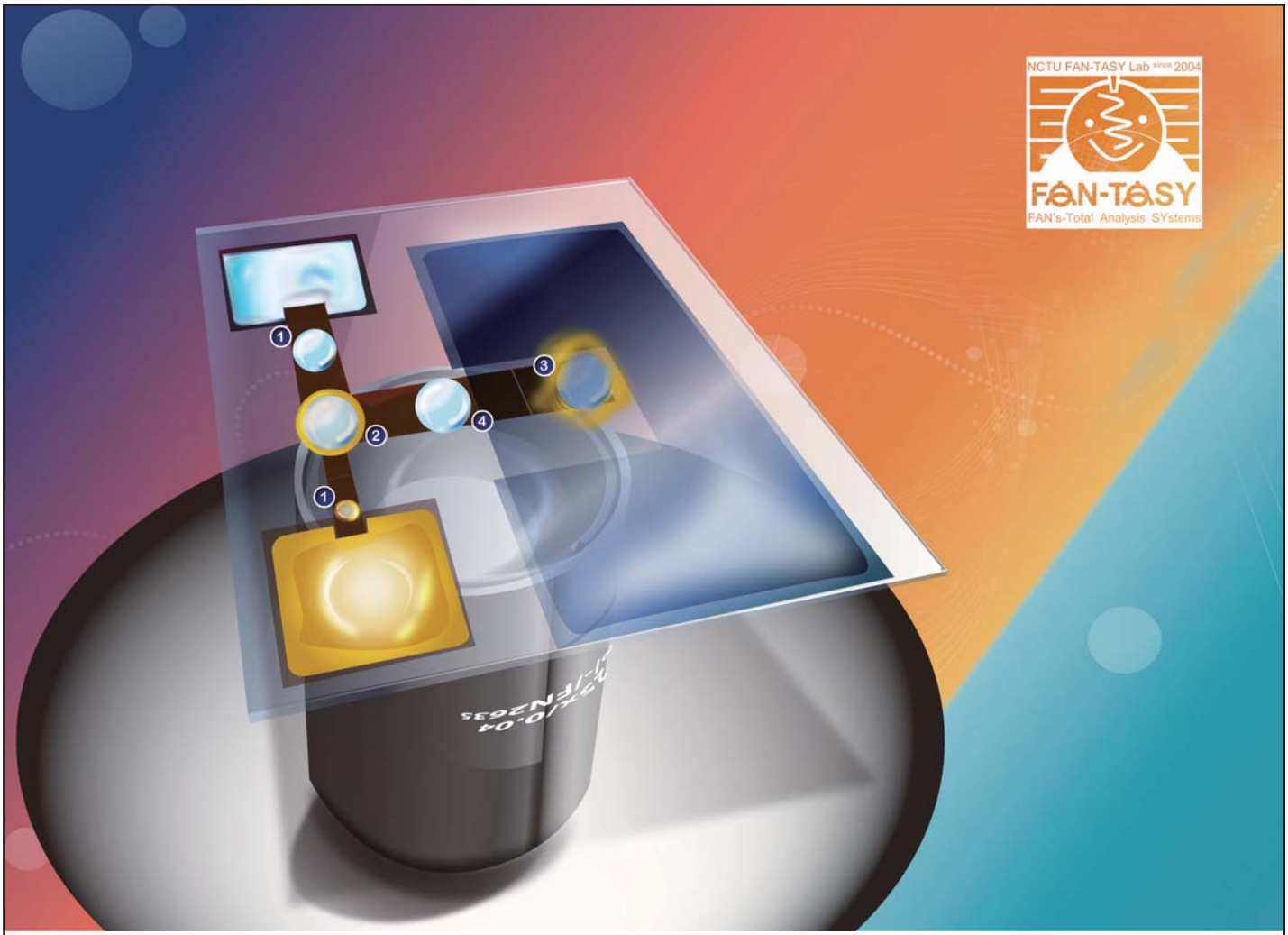

Featuring work from the FAN-TASY laboratory of Prof. Shih-Kang Fan in collaboration with Prof. Chiun-Hsun Chen at National Chiao Tung University, Taiwan

Title: Encapsulated droplets with metered and removable oil shells by electrowetting and dielectrophoresis

An encapsulated droplet with an adjustable water-to-oil volume ratio and a further removable oil shell is demonstrated through the steps of (1) generation, (2) encapsulation, (3) rinsing, and (4) emersion. This technique would enhance digital microfluidics by facilitating fluidic manipulation, reducing biofouling, decreasing core evaporation, improving detection signal-to-noise ratio, and simplifying device packaging.

As featured in:

See Shih-Kang Fan *et al.*, *Lab Chip*, 2011, **11**, 2500.

RSC Publishing

www.rsc.org/loc

Registered Charity Number 207890

Lab on a Chip

Dynamic Article Links

Cite this: *Lab Chip*, 2011, **11**, 2500

www.rsc.org/loc

PAPER

Encapsulated droplets with metered and removable oil shells by electrowetting and dielectrophoresis†

Shih-Kang Fan,*[ab] Yao-Wen Hsu[b] and Chiun-Hsun Chen[b]

Received 19th February 2011, Accepted 13th May 2011
DOI: 10.1039/c1lc20142e

A water-core and oil-shell encapsulated droplet exhibits several advantages including enhanced fluidic manipulation, reduced biofouling, decreased evaporation, and simplified device packaging. However, obtaining the encapsulated droplet with an adjustable water-to-oil volume ratio and a further removable oil shell is not possible by reported techniques using manual pipetting or droplet splitting. We report a parallel-plate device capable of generation, encapsulation, rinsing, and emersion of water and/or oil droplets to achieve three major aims. The first aim of our experiments was to form encapsulated droplets by merging electrowetting-driven water droplets and dielectrophoresis-actuated oil droplets whose volumes were precisely controlled. 25 nL water droplets and 2.5 nL non-volatile silicone oil droplets with various viscosities (10, 100, and 1000 cSt) were individually created from their reservoirs to form encapsulated droplets holding different water-to-oil volume ratios of 10 : 1 and 2 : 1. Secondly, the driving voltages, evaporation rates, and biofouling of the precise encapsulated droplets were measured. Compared with the bare and immersed droplets, we found the encapsulated droplets (oil shells with lower viscosities and larger volumes) were driven at a smaller voltage or for a wider velocity range. In the dynamic evaporation tests, at a temperature of 20 ± 1 °C and relative humidity of $45 \pm 3\%$, 10 cSt 10 : 1 and 2 : 1 encapsulated droplets were moved at the velocity of 0.25 mm s^{-1} for 22 and 35 min until losing 16.6 and 17.5% water, respectively, while bare droplets followed the driving signal for only 6 min when 11.4% water was lost. Evaporation was further diminished at the rate of 0.04% min^{-1} for a carefully positioned stationary encapsulated droplet. Biofouling of 5 μg ml^{-1} FITC-BSA solution was found to be eliminated by the encapsulated droplet from the fluorescent images. The third aim of our research was to remove the oil shell by dissolving it in an on-chip rinsing reservoir containing hexane. After emersion from the rinsing reservoir, the bare droplet was restored as hexane rapidly evaporated. Removal of the oil shell would not only increase the evaporation of the core droplet when necessary, but also enhance the signal-to-noise ratio in the following detection steps.

Introduction

Since the first demonstration of reconfigurable droplet driving by electrowetting[1] or electrowetting-on-dielectric (EWOD),[2] digital microfluidics (DMF)[3,4] has grown rapidly in the past decade, both through academic research on biochemical assays[5] and industrial prototyping for point of care tests.[6] For the ability to control individual droplets on a programmable electrode array, electrowetting provides reconfigurability, flexibility, and portability to perform on-chip chemical and biomedical protocols for DNA,[7,8] protein,[9,10] and cell analysis.[11,12] All sophisticated procedures were established based on several milestones of DMF, including basic droplet functions (creating, transporting, splitting, and merging),[13] droplet mixing,[14] driving of various fluids,[15–17] and anti-biofouling.[18,19]

In many DMF studies, silicone oil is used as a filler fluid to surround the immiscible aqueous droplets and fill the empty space between a pair of parallel plates where electrowetting electrodes are deposited and patterned. Compared with pumping bare droplets in an air environment, the filler silicone oil increases the contact angle change by electrowetting for reduced interfacial tension according to the Lippmann–Young equation.[20] It also decreases the threshold voltage as the contact angle hysteresis and counter-line friction of water are lowered.[4,21] In

[a]*Department of Materials Science and Engineering, National Chiao Tung University, 207, Engineering 1, 1001 University Road, Hsinchu, Taiwan. E-mail: skfan@mail.nctu.edu.tw; Fax: +886-3-5729912; Tel: +886-3-5712121 ext. 55813*

[b]*Department of Mechanical Engineering, National Chiao Tung University, Hsinchu, Taiwan*

† Electronic supplementary information (ESI) available: The plotted curves (Fig. S1) and captured images (Table S1) of the static evaporation of the 2 : 1 W/O droplets whose core water droplets were not carefully positioned; formation of a 10 cSt 2 : 1 W/O droplet (Video 1); generation, encapsulation, rinsing, and emersion of a 10 cSt 10 : 1 W/O droplet (Video 2); droplet breaking of a 1000 cSt 2 : 1 W/O droplet (Video 3). See DOI: 10.1039/c1lc20142e

addition, a thin silicone oil film between the aqueous droplet and the solid surfaces of the device was reported to minimize the biomolecular adsorption (*i.e.*, biofouling).[4,15] Certainly, the silicone oil prevents evaporation, which is especially important for tiny aqueous droplets with a high surface-to-volume ratio.[4,15] However, the supplemented silicone oil prohibits the usage of miscible solvents, such as hexane, used to dissolve silicone oil in this article. The filler fluid also brings some disadvantages at the device or system level. By using the silicone oil as the filler fluid, packaging of the parallel plate devices without oil leakage becomes more complicated. Designing a leakage-free modular interface[22] to transport droplets between two oil-filled devices would be another challenge. Furthermore, in a well-packaged device, it is difficult to arbitrarily add or remove aqueous liquids when a given inter-plate fluidic space is pre-loaded with a certain amount of oil.

Recently, water-core and oil-shell encapsulated droplets have been demonstrated as an alternative to DMF.[23–26] The oil shell of the encapsulated droplet should preserve the similar aforementioned advantages of the filler oil, such as enhanced fluidic manipulation, reduced biofouling, and decreased evaporation. Without filling the entire inter-plate fluidic space with water and oil, the encapsulated droplets simplify the device packaging, modular interface, and fluid addition and removal. Currently, the encapsulated droplets are prepared by two means: (1) manually pipetting water and oil droplets at a certain ratio[23,24] and (2) electrically splitting from a reservoir containing water and oil, *i.e.*, a larger encapsulated droplet.[25,26] However, the two methods are unable to create a tiny encapsulated droplet with a precise water-to-oil volume ratio. For further applications of encapsulated droplets to lab-on-a-chip (LOC), predictable performances based on metered water and oil are desirable.

In this article, we present a reconfigurable and reproducible procedure to form encapsulated droplets by merging water and oil droplets individually created in advance by EWOD and dielectrophoresis (DEP), respectively. With reliable water-to-oil volume ratios, the advanced DMF functions of encapsulated droplets were performed and characterized with their driving voltages, evaporation rates, and preliminary results of biofouling. The metered oil shell is further removable, which is essential to achieve rapid evaporation or to obtain clear detection signals, without noise from the oil shell. For example, in proteomics analyses using MALDI-MS (matrix assisted laser desorption/ionization-mass spectrometry), the sample purification and/or preparation would be performed in encapsulated droplets with precise water-to-oil volume ratios. The oil shell would be subsequently removed for rapid evaporation and enhanced MALDI-MS signals without interferences caused by oil.[9,27,28]

We regard the addition and removal of quantitative oil shells as another milestone of DMF. In addition to the aforementioned advantages of encapsulated droplets, the presented technique handles not only aqueous and oil (or non-polar organic) droplets but also molecules arranged along or transported across the water–oil interface. Therefore, the platform could be further applied to artificial bilayer lipid membrane (BLM) formation,[29–32] extraction,[33–35] synthesis,[36] and crystallization,[37–40] currently examined in a continuous segmented multiphase flow or in a bulk filler oil medium.

Design and principle

In this section, we describe the formation of encapsulated droplets, which is defined as pipetting, splitting, and merging. The design and principle of the formation of encapsulated droplets by merging are detailed.

Encapsulated droplet formation by pipetting

Encapsulated droplets can be simply formed by manual pipetting.[23,24] We began our studies with the pipetted encapsulated droplet having different oil volumes and viscosities in a 300 μm gap between parallel plates, and investigated the aspects of the threshold EWOD driving voltage, splitting voltage, and evaporation rate.[23] The viscosity and volume of the oil shell did directly influence the driving voltage and evaporation rate. However, because of the low surface tension (~20 mN m^{-1}, viscosity dependent) of silicone oil, dispensing a quantified oil droplet without residues left on the pipette tip was difficult. After dispensing, we needed to calibrate the oil volume from its weight and optical geometry. In real applications, programmable generation of precise encapsulated droplets by droplet splitting or merging on a DMF chip is more desirable.

Encapsulated droplet formation by splitting

Firstly, Fig. 1(a) illustrates two daughter encapsulated droplets formed by splitting. The water-to-oil volume ratios of the two daughter encapsulated droplets would be close if even splitting is performed, without satellite oil droplets commonly seen in early works.[17,23,25] Secondly, as sketched in Fig. 1(b), an encapsulated droplet can be generated from a reservoir containing water and oil, or a larger encapsulated droplet. As previously reported, the generated encapsulated droplets exhibited different oil volumes depending on the splitting conditions, *i.e.*, applied voltage.[25] Thirdly, an encapsulated droplet can be formed by emersion and splitting of a water droplet from an oil reservoir (Fig. 1(c)). As shown in Fig. 1(d)–(i), a water droplet (Fig. 1(d)) was driven by EWOD in a 100 μm gap between parallel plates to contact a 100 cSt silicone oil reservoir. The oil spontaneously encapsulated the water droplet (Fig. 1(e)), and was then stretched out as the water droplet moved to the right (Fig. 1(f)). As the water droplet was pumped further, the protruded oil necked down (Fig. 1(g)) and finally broke to form an encapsulated droplet with some satellite oil droplets left behind (Fig. 1(h)). As shown in Fig. 1(i), the encapsulated droplet was successfully generated and manipulated. However, because the necking and breaking of the oil shell was not well controlled, the emersion and splitting processes did not provide an encapsulated droplet with a precise water-to-oil volume ratio.

Encapsulated droplet formation by merging

Instead of pipetting and splitting, merging provides a better approach to obtaining precise encapsulated droplets. Previously, we have reported a general DMF platform employing EWOD and DEP to manipulate conductive (water) and dielectric (silicone oil, decane, and hexadecane) droplets manually pipetted between parallel plates.[17] The DEP-driven oil droplet encapsulated the EWOD-addressed water droplet to form an encapsulated

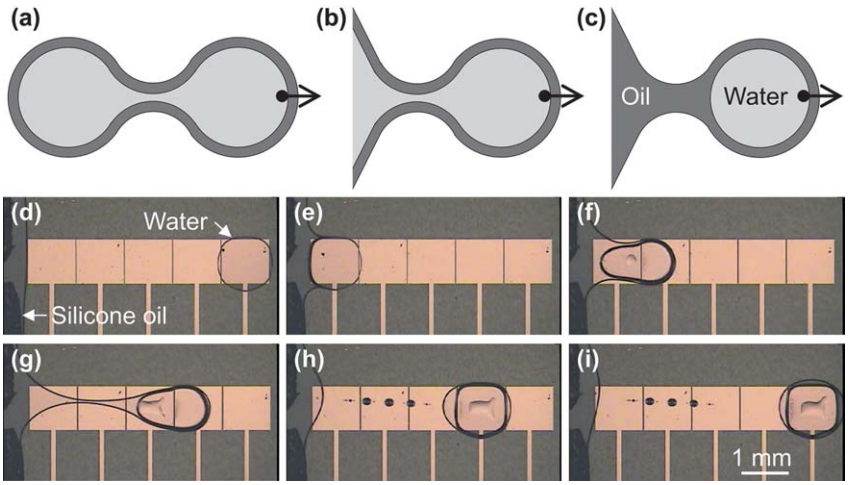

Fig. 1 Encapsulated droplet formation by splitting. (a) Even splitting. (b) Splitting from a larger encapsulated droplet (reservoir). (c) An encapsulated droplet generated by emersion and splitting. The procedure of emersion and splitting of a water droplet from an oil reservoir is shown in (d)–(i).

(water-core/oil-shell or W/O) droplet with a 1 : 1 water-to-oil volume ratio (named 1 : 1 W/O droplet hereafter). Based on that study, here we designed a new parallel-plate device to (1) generate oil and water droplets with precise volumes, (2) form encapsulated droplets with desired water-to-oil volume ratios by merging, and (3) remove the oil shell when needed.

A parallel-plate device was designed for the encapsulated droplet experiments as shown in Fig. 2. The device was equipped with three reservoirs: a water reservoir (shown W Res. in Fig. 2), an oil reservoir (O Res.), and a rinsing reservoir (R Res.). The water and oil reservoirs provided the core and shell liquids for the encapsulated droplets, respectively, while the rinsing reservoir contained a rinsing liquid, hexane, to dissolve and remove the silicone oil shell. As indicated by the numbers shown in Fig. 2, there were four main stages of the manipulated droplets: (1) generation of oil (O) and water (W) droplets, (2) encapsulation to form the W/O droplet, (3) rinsing the oil shell in the rinsing reservoir, and (4) emersion of the water droplet from the rinsing reservoir. The bottom plate contained several driving electrodes covered by dielectric and hydrophobic layers, while a common electrode was deposited on the top plate and coated with a hydrophobic material. When proper electric signals were applied between the common and driving electrodes, EWOD and/or DEP occurred to perform the droplet functions. To hold the rinsing liquid in the rinsing reservoir area, a capillary enhancer was placed on the top plate to reduce the gap height and increase the capillary force.

The EWOD force, F_{EWOD}, the force driving the water droplet in a parallel plate device can be derived from the Laplace–Young and the Young–Lippmann equations:

$$F_{EWOD} = \frac{\varepsilon_0 \varepsilon_D W_{EWOD}}{2t} V^2, \quad (1)$$

where ε_0 is the permittivity of vacuum, ε_D and t (shown in Fig. 2 (b)) are the permittivity and thickness of the dielectric/Teflon layer, W_{EWOD} is the width of the EWOD driving electrode, V is the voltage across the dielectric/Teflon layer. The value of V varies depending on the frequency of the applied signal as we reported previously.[12,42]

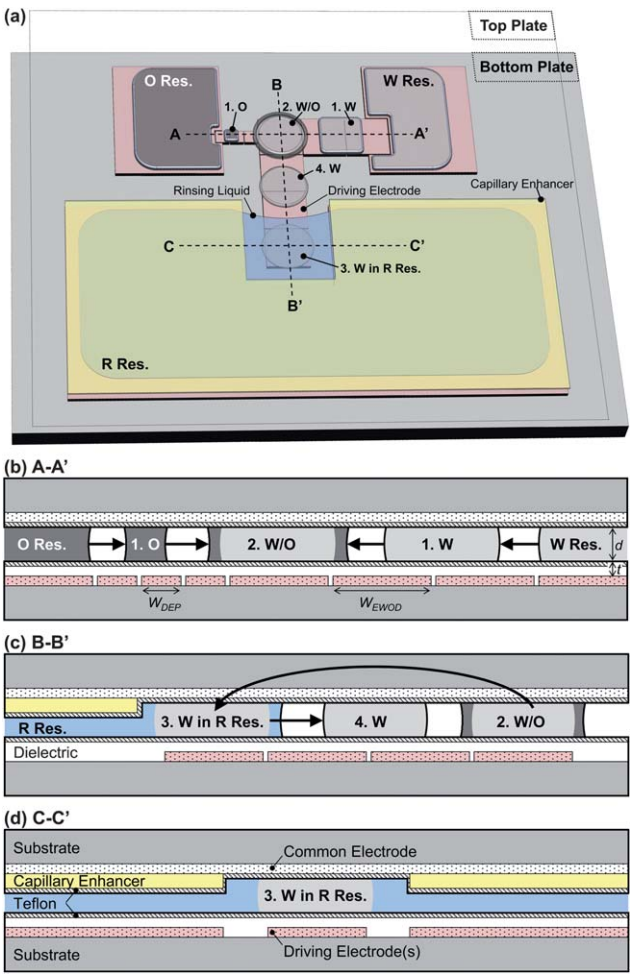

Fig. 2 Configuration of the designed parallel-plate device having water, oil, and rinsing reservoirs to perform the four main stages of droplet (1) generation, (2) encapsulation, (3) rinsing, and (4) emersion.

The DEP force, F_{DEP}, the force used to create and transport oil droplets is described as:[17]

$$F_{DEP} = \frac{\varepsilon_0 \varepsilon_D W_{DEP}}{2} V^2 \left(\frac{\varepsilon_{Oil}}{\varepsilon_{Oil} t + \varepsilon_D d} - \frac{\varepsilon_{Air}}{\varepsilon_{Air} t + \varepsilon_D d} \right), \quad (2)$$

where W_{DEP} is the width of the DEP driving electrode, V is the externally applied voltage, ε_{Oil} and ε_{Air} are the permittivities of oil and air, respectively, and d (Fig. 2(b)) is the distance between the parallel plates. The area of the DEP driving electrode was designed one tenth of the EWOD driving electrode. As a result, the volume of the DEP-generated oil droplet was one tenth of the EWOD-generated water droplet. By merging an oil droplet with a water droplet, an encapsulated droplet with the water-to-oil volume ratio of 10 : 1 (*i.e.*, 10 : 1 W/O droplet) was obtained. Similarly, different volume ratios, *e.g.*, 10 : 2, 10 : 3, *etc.*, were possible by merging a water droplet with multiple oil droplets. Different electrode sizes together with various water/oil droplet number combinations make the presented scheme flexible to provide almost any encapsulated droplet.

Experimental section

Parallel-plate device, system, and materials

Using the device design shown in Fig. 2, we fabricated a parallel-plate device whose EWOD driving electrodes were 1 mm × 1 mm, and DEP driving electrodes were 316 μm × 316 μm. With 25 μm thick spacers placed between the plates, the volume of a single EWOD-created DI (deionized) water droplet was 25 nL, and a DEP-created silicone oil droplet was 2.5 nL. The EWOD and DEP driving electrodes and reservoir electrodes were patterned on the bottom glass plate by wet etching of deposited Cu/Ti (200 nm/20 nm) or ITO (indium tin oxide, 200 nm).[12,17,22,41] Subsequently, a 1.1 μm thick SU-8 (SU-8 2002, MicroChem) dielectric layer was spun on the bottom plate with etched electrodes. The SU-8 surface was then coated with a 55 nm thick Teflon (AF 1600, DuPont) layer by spin coating to finish the process of the bottom plate. The top glass plate contained an unpatterned ITO layer as a transparent common electrode. A 10 μm thick photoresist layer, AZ P4620 (Clariant), was patterned by photolithography on top of the ITO layer for holding the rinsing solvent by capillary force in the decreased gap (*i.e.*, 15 μm) between plates in the rinsing reservoir area. Finally, a 55 nm thick Teflon layer was coated to make the surface of the top plate hydrophobic.

Before our experiments, the common electrode on the top plate was connected to the electric ground potential. The contact pads of the driving and reservoir electrodes on the bottom plate were connected to the common terminals of SPDT (single pole double throw) relays (LU-5, Rayex Electronics). The electric potential of the electrodes was switched by the relays between the electric ground and high potentials. AC or DC electric high potential was generated from a function generator (33210A, Agilent Technologies) and amplified through an amplifier (A-304, A. A. Lab Systems). The relays were switched by the digital output signals of a data acquisition device (USB-6251, National Instruments) programmed by LabVIEW software.

Adequate DI water and silicone oil were dispensed on the bottom plate. Silicone oil with different viscosities (10, 100, and 1000 cSt (DMS-T11, T21, T31, Gelest Inc.)) were tested. It is noteworthy that the evaporation rate of low viscosity silicone oils, commonly used in DMF devices,[1,4,25] is quite high. For example, the vapor pressure of 1 cSt silicone oil is 4 mm Hg at 25 °C (datasheet, Gelest Inc). To perform reliable experiments, we used 10, 100, and 1000 cSt silicone oils whose evaporation are negligible from datasheets and experiments. The top and bottom plates were then assembled with 25 μm high spacers in between. Because hexane, the rinsing liquid, is highly volatile (vapor pressure of 73 mm Hg at 25 °C), it was injected between the plates and drawn by capillarity to its reservoir when the oil shell needed to be removed. The assembled devices were placed on an inverted fluorescent microscope (Olympus, IX71 with DP30BW cooled CCD camera) or a custom-made observation system equipped with imaging lenses (Optem, Zoom 125) and a color CCD camera (Sony, SSC-DC50A).

In addition to using DI water as the core droplet, a protein solution was employed for biofouling investigations. 5 μg ml^{-1} FITC-BSA (fluorescein isothiocyanate labeled bovine serum albumin, Sigma Chemical) solution was prepared in 10 mM Tris-HCl (pH 7.8) buffer containing 0.1 mM sodium azide buffer.

Generation (stage 1)

After assembly, electric signals were applied to hold the silicone oil and DI water in their own reservoir areas as shown in Fig. 3 (a). We used DC signals to generate DEP on oil and AC 1 kHz square wave signals to generate EWOD on water. By properly and sequentially applying sufficient voltage at 240 V_{DC} on the oil reservoir electrode and the DEP driving electrodes, silicone oil was drawn from its reservoir, and then a 2.5 nL and 10 cSt silicone oil droplet was generated (Fig. 3(b)). The generation process was repeated five times as shown in Fig. 3(b)–(f). A 12.5 nL oil droplet was formed by merging the five oil droplets on a larger EWOD electrode as shown in Fig. 3(g). Here we clarify that DEP and EWOD driving electrodes were used to indicate smaller (316 μm × 316 μm) and larger (1 mm × 1 mm) electrodes for oil and water droplet generations. When applying DC voltage on the larger electrode, DEP can be used to hold the 12.5 nL oil droplet. As shown in Fig. 3(h), a 25 nL water droplet was then created by EWOD when applying a 1 kHz and 48 V_{RMS} AC signal. The generation procedure can be seen in Video 1 in the ESI.†

The volume variation of the five generated oil droplets was analyzed optically from Fig. 3(b)–(f) using image processing software (Vision 8.0, National Instruments). The standard deviation of the oil volume was negligible (2.5 pL), meaning the oil droplet generation was repeatable. However, the average volume of oil droplets was 3.06 nL, 22% larger than the designed volume determined by the DEP driving electrode. The water droplet volume measured 25.88 nL. To attain more precise droplet volumes, a feedback control scheme would be adopted in the future.[42] For simplifying the description throughout the article, we use the designed volume instead of the real volume of the droplets.

Encapsulation (stage 2)

The encapsulated droplet was formed by merging the two created and metered oil and water droplets. As shown in Fig. 3

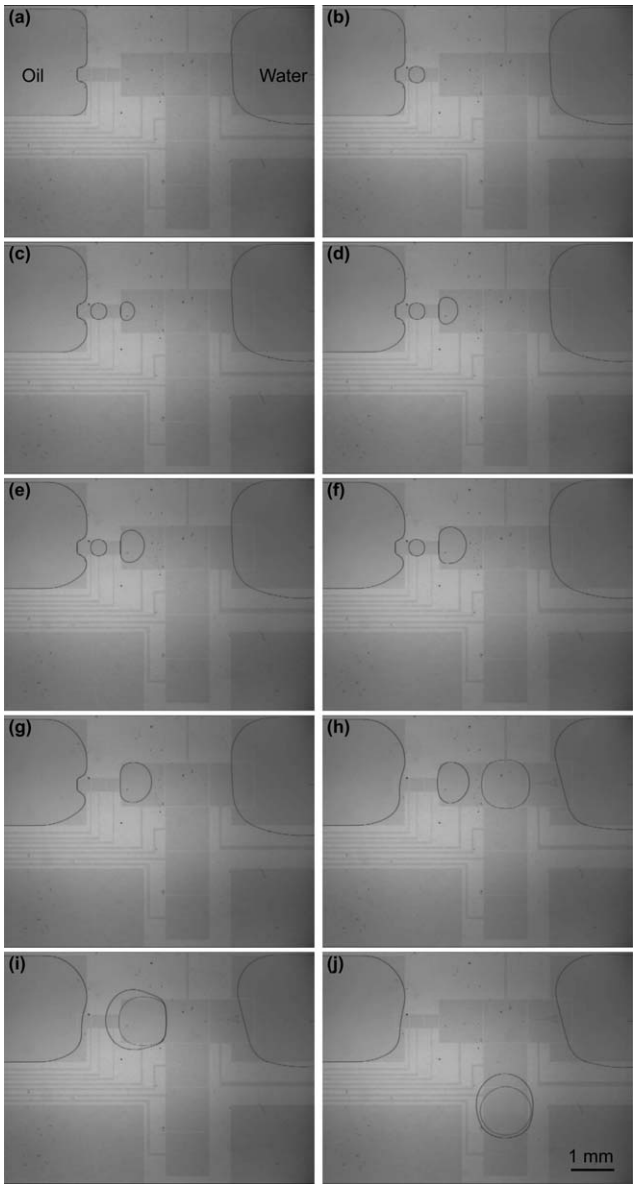

Fig. 3 Encapsulated droplet formation by droplet generating and merging. (a) 10 cSt silicone oil (left) and water (right) reservoirs were positioned by EWOD and DEP, respectively. (b)–(g) Five 2.5 nL oil droplets were generated and merged into a 12.5 nL oil droplet by DEP. (h) A 25 nL water droplet was generated by EWOD. (i) A 2 : 1 W/O droplet was formed by merging. (j) The encapsulated droplet was pumped by EWOD. See Video 1 in the ESI.†

(i), after merging, the 12.5 nL oil droplet spontaneously encapsulated the 25 nL water droplet to form a 2 : 1 W/O droplet. The encapsulated droplet was pumped by EWOD as shown in Fig. 3(j). We further evaluated the pumping voltage and evaporation of the created encapsulated droplets with different water-to-oil volume ratios (10 : 1 and 2 : 1) using silicone oil with viscosities of 10, 100, and 1000 cSt, which will be presented in the discussion section. Furthermore, we preliminarily tested biofouling using bare and encapsulated (10 cSt 10 : 1 W/O) droplets containing 5 μg ml^{-1} FITC-BSA in the water droplets.

Rinsing and emersion (stage 3 and 4)

The removal of the oil shell is more challenging than the addition. Previously, we used DEP and EWOD forces to split an encapsulated droplet.[17] However, because of the strong interfacial tension between water and oil (43 mN m^{-1} measured by the pendent drop method), completely separating the water-core and oil-shell by physical forces was difficult. Here we develop a chemical approach to this issue by dissolving silicone oil in a non-polar solution, hexane, which is immiscible to water. The interfacial tension between water and hexane (41 mN m^{-1}

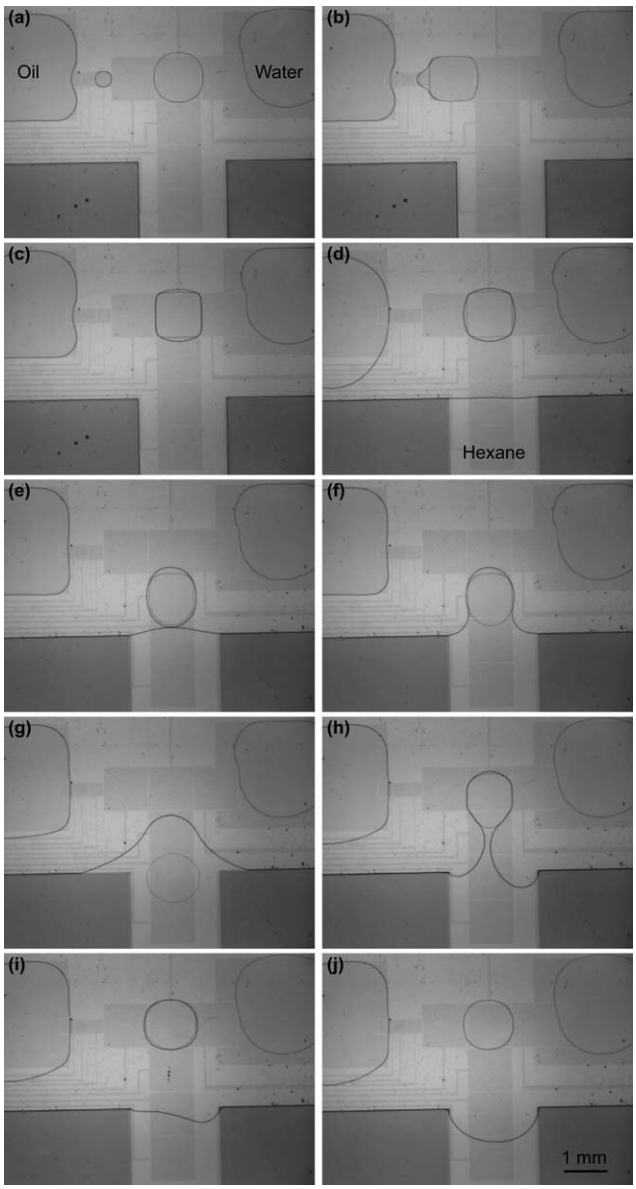

Fig. 4 Encapsulated droplet formation and oil shell removal. (a) A 2.5 nL 10 cSt silicone oil droplet and a 25 nL water droplet were generated. (b)–(c) A 10 : 1 W/O droplet was formed and pumped. (d) The rinsing solvent, hexane, was injected. (e)–(g) The droplet was immersed and pumped in the rinsing reservoir. (h) The droplet emerged. (i) The water droplet was wrapped with a thin hexane shell. (j) The water droplet was recovered after hexane evaporation. See Video 2 in the ESI.†

measured by the pendent drop method) was close to that between water and oil.

As shown in Fig. 4 and Video 2 in the ESI,† a 2.5 nL 10 cSt silicone oil droplet and a 25 nL water droplet were created (Fig. 4 (a)) and merged (Fig. 4(b)) to form a 10 : 1 W/O droplet. The encapsulated droplet was moved by EWOD as shown in Fig. 4 (c). Before removing the 2.5 nL oil shell, hexane was injected between the top and bottom plates. Because of the capillary enhancer made of 10 μm thick AZ P4620, hexane was maintained in its reservoir area as shown in Fig. 4(d). The encapsulated droplet was then moved down (Fig. 4(e)) to touch (Fig. 4(f)) and immerse into (Fig. 4(g)) the rinsing reservoir. Once the silicone oil shell contacted with the hexane, it mixed and dissolved in the hexane. The water droplet was driven back and forth by EWOD in the rinsing reservoir for 1 min to enhance mixing and ensure the silicone oil (from 2.5 to 12.5 nL) was completely dissolved and diffused in the hexane, assisted by the shear force. The water droplet emerged from the rinsing reservoir (Fig. 4(h)) to form another encapsulated droplet wrapped by a thin hexane shell as shown in Fig. 4(i). As described above, the hexane shell volume was not easily quantified through the emersion and splitting process (Fig. 1(c)–(i)). Due to hexane being highly volatile, the hexane shell evaporated in 30 s to restore the original bare water droplet as shown in Fig. 4(j).

Discussion

Driving voltage of encapsulated droplets

With 1 mm × 1 mm EWOD electrodes and 316 μm × 316 μm DEP electrodes, 25 nL DI water droplets and 2.5 nL oil droplets were individually generated in the 25 μm high gap between the parallel plates by applying 48 V_{RMS} and 240 V_{DC}, respectively. To test their DMF functions, we prepared encapsulated droplets with two water-to-oil volume ratios of 10 : 1 and 2 : 1 using silicone oils whose viscosities were 10, 100, and 1000 cSt. We recorded the minimum required voltage to move the encapsulated droplet back and forth at least once on five driving electrodes (1 mm × 1 mm). Each of the driving electrodes was powered for a certain switching time (ST), from 1 to 64 s, to move the droplet at the velocity of 1/ST (mm s^{-1}). The average voltages from at least three experiments of each condition are listed in Table 1. For comparison purposes, bare water droplets in air and immersed water droplets in different filler oil environments were also tested. In some cases, the droplet broke up during experiments. Among them, some droplet fragmentations were not severe, so the remaining droplet still completed the pumping procedure. As shown in the inset of Fig. 5 and Video 3 in the ESI,† the 1000 cSt 2 : 1 W/O droplet was about to break when it was driven with the switching time of 32 s. The volume of the remaining droplet was sufficient to finish the pumping procedure back and forth on the five driving electrodes. For those cases, we averaged the required voltage and they are noted with a superscript "a" in Table 1. In the rest of the droplet breaking cases, the fragmentation stopped the droplet following the driving signals so that the droplet did not complete the pumping procedure, and these are indicated with a superscript "b". In addition to droplet

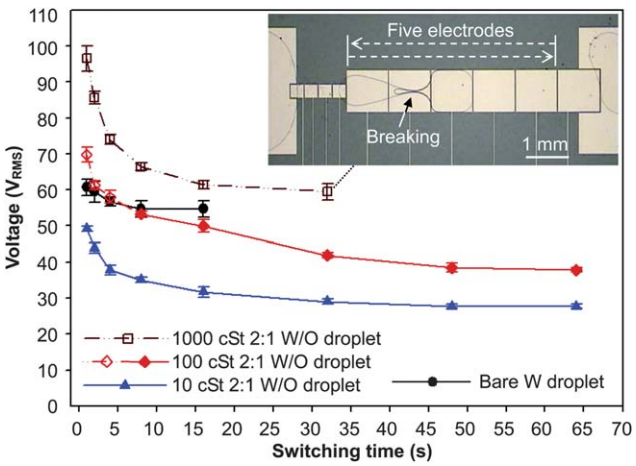

Fig. 5 Minimum driving voltages of successful cases (solid symbols) and droplet breaking but completion cases (hollow symbols) of bare and encapsulated droplets. One case where the droplet fragmented but completed pumping (1000 cSt 2 : 1 W/O droplet) is shown in the inset and Video 3 in the ESI.†

Table 1 The minimum required driving voltage of a 25 nL water droplet to move back and forth once on five 1 mm × 1 mm electrode by sequentially turning on each electrode for a certain switching time (ST). (a) Encapsulated droplets containing silicone oil with different volumes and viscosities, (b) immersed water droplets in filler silicone oil, and (c) bare water droplets are tested

	(a) Voltage of encapsulated droplets with different water-to-oil volume ratios (V_{RMS})						(b) Voltage of immersed droplets (V_{RMS})			(c) Voltage of bare droplets (V_{RMS})
	10 cSt		100 cSt		1000 cSt					
ST (s)	10 : 1	2 : 1	10 : 1	2 : 1	10 : 1	2 : 1	10 cSt	100 cSt	1000 cSt	
1	45.8	49.2	N/A[b]	69.8[a]	N/A[b]	96.5[a]	60.1[a,b]	N/A[b]	N/A[b]	60.7
2	41.8	43.9	N/A[b]	61.3[a]	N/A[b]	85.6[a]	46.2	N/A[b]	N/A[b]	59.4
4	36.7	37.8	62.8[a,b]	58.0[a]	N/A[b]	73.9[a]	43.5	N/A[b]	N/A[b]	56.7
8	35.1	35.1	56.8[a,b]	53.3	N/A[b]	66.4[a]	34.3	N/A[b]	N/A[b]	54.7
16	30.7	31.7	52.7[a,b]	50.0	N/A[b]	61.4[a]	28.7	N/A[b]	N/A[b]	54.7
32	29.1	29.0	43.8	41.8	N/A[b,c]	59.5[a]	23.9	47.3	N/A[b]	N/A[c]
48	25.9	27.7	37.3	38.5	N/A[c]	N/A[c]	21.5	41.3	N/A[b]	N/A[c]
64	24.7	27.7	37.0	37.8	N/A[c]	N/A[c]	19.7	38.8	N/A[b]	N/A[c]

[a] Droplet breaking but completion of the pumping procedure; see Video 3 in the ESI.† [b] Droplet breaking and non-completion of the pumping procedure. [c] Droplet evaporation and non-completion of the pumping procedure.

breaking, some droplets did not complete the pumping procedure because of evaporation, which are noted with a superscript "c" in Table 1. The driving voltages of the successful cases without droplet breaking are shown as solid symbols in Fig. 5, while those of the breaking but completing cases are show in hollow symbols. From Table 1 and Fig. 5, there are several findings:

1. Encapsulated or immersed droplets required lower driving voltages than bare water droplets in air for all the successful cases. It was because the contact angle change was enhanced, and the interfacial tension and contact angle hysteresis were lowered.[4,21]

2. Lower oil viscosity decreased the driving voltage for both encapsulated and immersed droplets. The resistive forces of a droplet included counter-line friction, hysteresis force, and friction drag (or shear force caused by viscous effect).[43,44] The friction drag, proportional to the viscosity and velocity, was markedly reduced when the oil viscosity was low.

3. Encapsulated droplets were driven in a wider velocity range than the immersed ones. For immersed droplets, the droplet breaking was caused by the shear stress exerted at the water–oil interface when the oil viscosity and the water droplet velocity were sufficient. On the contrary, the shear stress and friction drag were reduced by the limited oil volume of the encapsulated droplets. Therefore, the encapsulated droplets required lower driving voltage than the immersed ones at high velocities. At low velocities, the counter-line friction and hysteresis force of the oil shell became dominant. Although the encapsulated droplets needed higher driving voltages at low velocities, they were successfully driven in a wider velocity range compared with the immersed ones.

4. The 10 : 1 W/O droplets were easier to break or stop than the 2 : 1 ones. Droplet breaking occurred when the resistive forces and the EWOD driving force were larger than the required breaking force. In the droplet breaking cases, the volume of the remaining droplet of a 2 : 1 W/O droplet was usually sufficient to complete the pumping procedure as shown in the inset of Fig. 5 and Video 3 in the ESI.† However, the 10 : 1 W/O droplets tended to stop after droplet breaking.

In summary, we found the encapsulated droplets having oil shells with lower viscosities and larger volumes were driven at a smaller voltage or for a wider velocity range compared with the bare and the immersed droplets.

Evaporation of encapsulated droplets

As highlighted by a superscript "c" in Table 1, evaporation hindered droplet pumping, especially for bare droplets and broken encapsulated droplets (*e.g.*, 1000 cSt). In the cases without droplet breaking, the encapsulated droplets (10 and 100 cSt) effectively suppressed the evaporation and endured a long-term operation time of up to 10 min when the switching time was 64 s. With the ability to form encapsulated droplets holding different water-to-oil volume ratios, the evaporation becomes adjustable to a necessary rate which is crucial to synthesis, crystallization, evaporation-related assembly, and other applications.[36–40] From Fick's law of diffusion, the theoretical evaporation rate of an concentric circular encapsulated droplet would be proportional to the molar diffusion rate (N) of water in the oil shell:[45]

$$N = \frac{2\pi dD}{\ln(r_{W/O}/r_W)}(C_{W,sW} - C_{W,sW/O}), \quad (3)$$

where d is the distance between the parallel plates and the thickness of the encapsulated droplet (Fig. 2(b)), D is the diffusion coefficient of water in silicone oil, $r_{W/O}$ and r_W are the radii of the W/O droplet and the W droplet, respectively, $C_{W,sW}$ and $C_{W,sW/O}$ are the water concentrations at the W droplet surface (water–oil interface) and at the W/O droplet surface (oil–air interface). From eqn (3), with the same water volume, the more the oil volume is (*i.e.*, greater $\ln(r_{w/o}/r_w)$), the less the evaporation rate will be. The influence of oil volume was first studied with bare water, 10 cSt 2 : 1 W/O, and 10 : 1 W/O droplets driven back and forth continuously on five driving electrodes at the center of 3 cm × 4 cm devices with a switching time of 4 s. The *dynamic evaporation* under the temperature of 20 ± 1 °C and the relative humidity (RH) of 45 ± 3% was evaluated by measuring the top-view area of the core water droplet using image processing software. The relative evaporation loss (V loss/V initial) until water loss stopped pumping is plotted against time in Fig. 6 (a) where each data point represents the average value of three measurements from at least 3 different experiments. After 6 min of pumping, the bare droplet lost 11.4% volume and stopped moving. 10 cSt 10 : 1 and 2 : 1 W/O droplets were pumped for 22 and 35 min when losing 16.6 and 17.5%, respectively. The lifetimes of the encapsulated droplets were extended not only by the slower evaporation rates but also by the smaller movable water volumes. In oil shells, the inertial force of the water droplet became more important because the counter-line friction and hysteresis force of the water droplet were reduced. The inertia pushed the core water droplet forward till the boundary of the powered electrode adjacent to a neighbour electrode even when the volume of the water droplet appeared not to be sufficient.

We also tested *static evaporation* of various droplets, including bare, immersed, encapsulated (10 cSt 2 : 1 W/O), and rinsed water droplets. With the same image processing method, we plotted the curves of relative evaporation loss against time in Fig. 6(b). Under the condition of 20 ± 1 °C and 48 ± 2% RH, a bare droplet entirely evaporated within 50 min (2.3% min^{-1}), while the evaporation of an immersed water droplet was negligible (0.1%) in the 150 min period. The insets of Fig. 6(b) show the evaporation procedure of an encapsulated droplet whose relative evaporation loss in 150 min was 6.2% at the rate of 0.04% min^{-1}. We noticed that the oil shell was not in a perfect circular shape for the counter-line friction and hysteresis force of oil. The non-uniform thickness of the oil shell caused uneven evaporation rates across the oil shell, which is different from the prediction of eqn (3) describing the evaporation of a concentric circular encapsulated droplet. In some of the experiments of the same 10 cSt 2 : 1 W/O droplets, once the core water droplet approached and touched the oil–air surface (Fig. S1 and Table S1 in the ESI†), the evaporation was 20 times higher at the rate of 0.88% min^{-1} which was even higher than the dynamic evaporation rate (0.5% min^{-1} from Fig. 6(a)). To better control the evaporation, it is important to form concentric circular and stationary

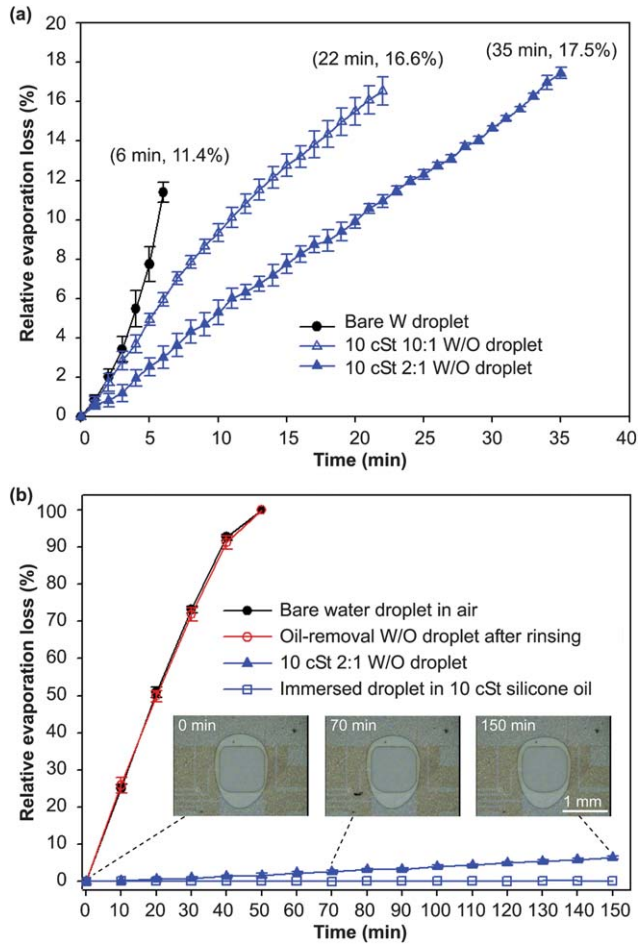

Fig. 6 Dynamic and static relative evaporation loss. (a) Dynamic evaporation by moving bare and encapsulated (10 cSt 10 : 1 and 2 : 1 W/O) droplets at 0.25 mm s^{-1} (switching time of 4 s) until stopped by evaporation. (b) Static evaporation of bare, rinsed, encapsulated (10 cSt 2 : 1 W/O shown in insets), and immersed water droplets.

encapsulated droplets between leveled plates to eliminate droplet moving caused by capillary and gravity effects.

Last but not least, the static evaporation of a 10 cSt 2 : 1 W/O droplet rinsed by hexane was recorded and plotted in Fig. 6(b). By comparing the evaporation curves of the bare and rinsed droplets, the oil shell was effectively removed through the rinsing and emersion step. Therefore, the oil shell would be put on when low evaporation and driving voltage are required during sample preparation and reaction. When rapid evaporation and enhanced signal-to-noise ratio (*e.g.*, mass spectrometry) are desirable,[9,27,28] the oil shell would be removed.

Biofouling

We preliminarily investigated biofouling using 10 cSt 10 : 1 W/O droplets with a protein solution core droplet containing 5 μg ml^{-1} FITC-BSA. The bare and encapsulated droplets were pumped back and forth between two electrodes with a switching time of 2 s and driving voltage of 67.7 V_{RMS} for 5 min as shown in Fig. 7 (a) and (c). Subsequently, the device was disassembled, and the droplets were removed. The surface of the bottom plate was

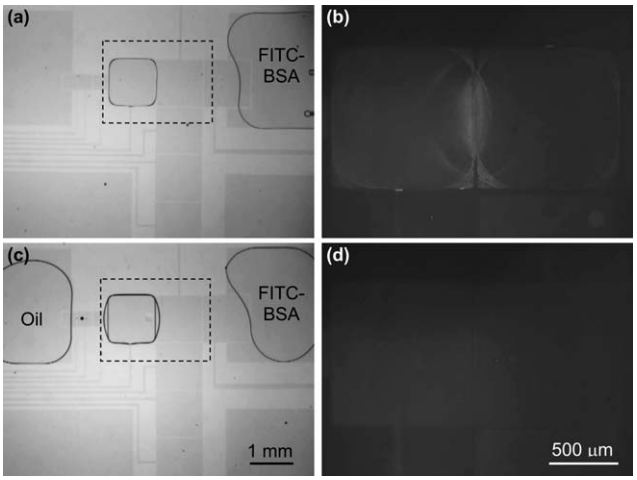

Fig. 7 Biofouling of 5 μg ml^{-1} FITC-BSA using bare and encapsulated droplets. (a) Transportation (67.7 V_{RMS}) of a bare droplet containing FITC-BSA back and forth on two driving electrodes within the dashed rectangle. (b) The fluorescent image of the dashed rectangle in (a) showing the adsorbed FITC-BSA on the two driving electrodes of the bottom plate after removing the bare droplet driven for 5 min. (c) A 10 cSt 10 : 1 W/O with a FITC-BSA solution core droplet pumped (67.7 V_{RMS}) between two electrodes within the dashed rectangle. (d) Biofouling of the encapsulated droplet after 5 min dirving was minimized from the fluorescent image of the dashed rectangle in (c).

inspected under a fluorescent microscope. Adsorption of FITC-BAS was found on the surface where the bare droplet was driven (Fig. 7(b)), while the biofouling was obviously reduced by the encapsulated droplet as shown in Fig. 7(d). More detailed and quantitative studies will be performed in the future on the presented device using varied protein concentrations, water-to-oil volume ratios, switching times, and applied voltages.

Conclusion

By merging water and oil droplets through EWOD and DEP, we formed encapsulated droplets containing removable oil shells with various volumes and viscosities. The performances of 10, 100, and 1000 cSt 10 : 1 and 2 : 1 W/O droplets were tested and compared with bare and immersed water droplets. The dynamic and static evaporation of the encapsulated droplet were evaluated. Biofouling of bare and encapsulated droplets was also tested. The presented DFM platform handling water and oil could be further applied to artificial BLM formation, extraction, synthesis, crystallization, and evaporation-related assembly.

Acknowledgements

This work was partially supported by the National Science Council, Taiwan, under grants NSC 98-2221-E-009-129-MY3 and NSC 99-2627-M-009-001.

Reference

1 M. G. Pollack, R. B. Fair and A. D. Shenderov, *Appl. Phys. Lett.*, 2000, **77**, 1725–1726.
2 J. Lee, H. Moon, J. Fowler, T. Schoellhammer and C.-J. Kim, *Sens. Actuators, A*, 2002, **95**, 259–268.
3 M. Abdelgawad and A. R. Wheeler, *Adv. Mater.*, 2009, **21**, 920–925.

4 R. B. Fair, *Microfluid. Nanofluid.*, 2007, **3**, 245–281.
5 L. Malic, D. Brassard, T. Veres and M. Tabrizian, *Lab Chip*, 2010, **10**, 418–431.
6 R. Sista, Z. Hua, P. Thwar, A. Sudarsan, V. Srinivasan, A. Eckhardt, M. Pollack and V. Pamula, *Lab Chip*, 2008, **8**, 2091–2104.
7 Y.-J. Liu, D.-J. Yao, H.-C. Lin, W.-Y. Chang and H.-Y. Chang, *J. Micromech. Microeng.*, 2008, **18**, 045017.
8 Y.-H. Chang, G.-B. Lee, F.-C. Huang, Y.-Y. Chen and J.-L. Lin, *Biomed. Microdevices*, 2006, **8**, 215–225.
9 A. R. Wheeler, H. Moon, C.-J. Kim, J. A. Loo and R. L. Garrell, *Anal. Chem.*, 2004, **76**, 4833–4838.
10 M. J. Jebrail and A. R. Wheeler, *Anal. Chem.*, 2009, **81**, 330–335.
11 I. Barbulovic-Nad, H. Yang, P. S. Park and A. R. Wheeler, *Lab Chip*, 2008, **8**, 519–526.
12 S.-K. Fan, P.-W. Huang, T.-T. Wang and Y.-H. Peng, *Lab Chip*, 2008, **8**, 1325–1331.
13 S. K. Cho, H. Moon and C.-J. Kim, *J. Microelectromech. Syst.*, 2003, **12**, 70–80.
14 P. Paik, V. K. Pamula and R. B. Fair, *Lab Chip*, 2003, **3**, 253–259.
15 V. Srinivasan, V. K. Pamula and R. B. Fair, *Lab Chip*, 2004, **4**, 310–315.
16 D. Chatterjee, B. Hetatothin, A. R. Wheeler, D. J. King and R. L. Garrell, *Lab Chip*, 2006, **6**, 199–206.
17 S.-K. Fan, T.-H. Hsien and D.-Y. Lin, *Lab Chip*, 2009, **9**, 1236–1242.
18 J.-Y. Yoon and R. L. Garrell, *Anal. Chem.*, 2003, **75**, 5097–5102.
19 V. N. Luk, G. C. H. Mo and A. R. Wheeler, *Langmuir*, 2008, **24**, 6382–6389.
20 M. Vallet, B. Berge and L. Vovelle, *Polymer*, 1996, **37**, 2465–2470.
21 H. J. J. Verheijen and M. W. J. Prins, *Langmuir*, 1999, **15**, 6616–6620.
22 S.-K. Fan, H. Yang and W. Hsu, *Lab Chip*, 2011, **11**, 343–347.
23 C.-W. Chen, Y.-W. Hsu, Y.-C. Chang, C.-H. Chen, and S.-K. Fan, *Proceeding of Asia-Pacific Conference on Transducers and Micro-Nano Technology*, Tainan, Taiwan, 2008, 136–139.
24 H.-C. Lin, Y.-J. Liu and D.-J. Yao, *Journal of the Association for Laboratory Automation*, 2010, **15**, 210–215.
25 D. Brassard, L. Malic, F. Normandin, M. Tabrizian and T. Veres, *Lab Chip*, 2008, **8**, 1342–1349.
26 R. Prakash and K. V. I. S. Kaler, *Lab Chip*, 2009, **9**, 2836–2844.
27 A. R. Wheeler, H. Moon, C. A. Bird, R. R. O. Loo, C.-J. Kim, J. A. Loo and R. L. Garrell, *Anal. Chem.*, 2005, **77**, 534–540.
28 H. Moon, A. R. Wheeler, R. L. Garrell, J. A. Loo and C.-J. Kim, *Lab Chip*, 2006, **6**, 1213–1219.
29 H. Bayley, B. Cronin, A. Heron, M. A. Holden, W. L. Hwang, R. Syeda, J. Thompson and M. Wallace, *Mol. BioSyst.*, 2008, **4**, 1191–1208.
30 K. Funakoshi, H. Suzuki and S. Takeuchi, *Anal. Chem.*, 2006, **78**, 8169–8174.
31 S. Aghdaei, M. E. Sandison, M. Zagnoni, N. G. Green and H. Morgan, *Lab Chip*, 2008, **8**, 1617–1620.
32 J. L. Poulos, W. C. Nelson, T.-J. Jeon, C.-J. Kim and J. J. Schmidt, *Appl. Phys. Lett.*, 2009, **95**, 013706.
33 H. Chen, Q. Fang, X.-F. Yin and Z.-L. Fang, *Lab Chip*, 2005, **5**, 719–725.
34 P. Mary, V. Studer and P. Tabeling, *Anal. Chem.*, 2008, **80**, 2680–2687.
35 N. A. Mousa, M. J. Jebrail, H. Yang, M. Abdelgawad, P. Metalnikov, J. Chen, A. R. Wheeler and R. F. Casper, *Science Translational Medicine*, 2009, **1**, 1–6.
36 A. Abou-Hassan, O. Sandre and V. Cabuil, *Angew. Chem., Int. Ed.*, 2010, **49**, 6288–6286.
37 B. Zheng, L. S. Roach and R. F. Ismagilov, *J. Am. Chem. Soc.*, 2003, **125**, 11170–11171.
38 L. Li, D. Mustafi, Q. Fu, V. Tereshko, D. L. Chen, J. D. Tice and R. F. Ismagilov, *Proc. Natl. Acad. Sci. U. S. A.*, 2006, **103**, 19243–19248.
39 B. Zheng, C. J. Gerdts and R. F. Ismagilov, *Curr. Opin. Struct. Biol.*, 2005, **15**, 548–555.
40 C. J. Gerdts, V. Tereshko, M. K. Yadav, I. Dementieva, F. Collart, A. Joachimiak, R. C. Stevens, P. Kuhn, A. Kossiakoff and R. F. Ismagilov, *Angew. Chem., Int. Ed.*, 2006, **45**, 8156–8160.
41 S.-K. Fan, W.-J. Chen, T.-H. Lin, T.-T. Wang and Y.-C. Lin, *Lab Chip*, 2009, **9**, 1590–1595.
42 J. Gong and C.-J. Kim, *Lab Chip*, 2008, **8**, 898–906.
43 V. Bahadur and S. V. Garimella, *J. Micromech. Microeng.*, 2006, **16**, 1494–1503.
44 H. Ren, R. B. Fair, M. G. Pollack and E. J. Shaughnessy, *Sens. Actuators, B*, 2002, **87**, 201–206.
45 F. P. Incropera and D. P. De Witt, in *Fundamentals of Heat and Mass Transfer*, John Wiley & Sons, 3rd edn, 1990, ch. 14, pp. 889–893.

